Journal of
Nuclear Engineering

MDPI

Article

The Effect of Ar and N_2 Background Gas Pressure on H Isotope Detection and Separation by LIBS

Indrek Jõgi *, Jasper Ristkok and Peeter Paris

Institute of Physics, University of Tartu, W. Ostwaldi Str. 1, 50411 Tartu, Estonia; jasper.ristkok@ut.ee (J.R.); peeter.paris@ut.ee (P.P.)
* Correspondence: indrek.jogi@ut.ee

Abstract: Laser-Induced Breakdown Spectroscopy (LIBS) is one candidate for analyzing the fuel retention in ITER plasma-facing components during maintenance breaks when the reactor is filled with near atmospheric pressure nitrogen or dry air. It has been shown that using argon flow during LIBS measurements increases the LIBS signal at atmospheric pressure conditions and helps to distinguish the hydrogen isotopes. However, atmospheric pressure might be suboptimal for such LIBS measurements. The present study investigated the effect of argon or nitrogen gas at different pressures on the hydrogen H_α line emission intensity during the LIBS measurements. Laser pulses with an 8 ns width were used to ablate a small amount of a molybdenum (Mo) target with hydrogen impurity. The development of the formed plasma plume was investigated by time- and space-resolved emission spectra and photographs. Photographs showed that the plasma plume development was similar for both gases, while the total intensity of the plume was higher in argon. Space-resolved emission spectra also had stronger H_α line intensities in argon. Shorter delay times necessitated the use of lower pressures to have sufficiently narrow lines for the distinguishing of the hydrogen isotopes. At the same line widths, the line intensities were higher at lower gas pressures and in argon. H_α and Mo I line emissions were spatially separated, which suggests that the geometry of collection optics should be considered when using LIBS.

Keywords: laser-induced breakdown spectroscopy; laser plasma plume; hydrogen isotope detection; plasma facing components

Citation: Jõgi, I.; Ristkok, J.; Paris, P. The Effect of Ar and N_2 Background Gas Pressure on H Isotope Detection and Separation by LIBS. *J. Nucl. Eng.* **2024**, *5*, 531–544. https://doi.org/10.3390/jne5040033

Academic Editor: Dan Gabriel Cacuci

Received: 13 September 2024
Revised: 5 November 2024
Accepted: 15 November 2024
Published: 22 November 2024

1. Introduction

The International Thermonuclear Experimental Reactor (ITER) is built with the aim of achieving the ignition of the deuterium–tritium (DT) fusion plasma and demonstrating the feasibility of fusion energy by achieving the value of an energy gain factor Q above 10. The operation of the ITER in the regime, which gives a great amount of fusion energy, results in the considerable retention of radioactive tritium fuel in the plasma-facing components of the reactor [1,2]. Therefore, the tritium inventory must be monitored to meet the safety requirements, and Laser Induced Breakdown Spectroscopy (LIBS) is a method that is considered a promising tool for this purpose [3,4]. LIBS uses short but powerful laser pulses to ablate a small amount of investigated material. The ablated material forms a transient plasma plume emitting light with a spectrum characteristic to the elements present in the investigated material. The usability of the method for the elemental analysis of plasma-facing components has been tested in several tokamaks [5–9] and numerous other studies [3,4].

The wavelength difference between hydrogen isotope lines is 0.06 nm for T_α and D_α and 0.18 nm for D_α and H_α. The distinguishing of these lines in the LIBS spectra requires sufficiently narrow linewidths. In the LIBS plasma, the width of hydrogen isotope lines is generally determined by Stark broadening related to the electron density [10]. This finding suggests that the LIBS spectra should be acquired at longer delay times after the laser pulse

when the electron density has become sufficiently small for distinguishing the lines of hydrogen isotopes. However, the intensity of the isotope lines also decreases at these delay times [11–13]. Furthermore, the linewidth and intensity values depend on many other parameters, including gas atmosphere and pressure [13–15]. The optimum conditions for isotopic line measurements may differ for each of these conditions.

In the ITER, the LIBS method is expectedly used for the tritium retention measurements during maintenance breaks when the vacuum vessel is at the atmospheric pressure [4]. In the case of atmospheric pressure nitrogen or air, the intensity of H_α line becomes too low at the delay times, where sufficiently narrow linewidths could be achieved, while the use of an Argon (Ar) atmosphere improves the intensity [12,15,16]. The Ar gas can be locally blown on the investigated sample surface, and the feasibility of this approach has been demonstrated in the Frascati Tokamak Upgrade (FTU) reactor using an LIBS system built on a robotic arm [7]. The system can also be used to make LIBS measurements at reduced pressures [7], which may allow higher hydrogen isotope line intensities at lower linewidth values [11].

In an earlier work, we used ns LIBS to investigate the time-dependent changes of hydrogen line intensities and linewidths in atmospheric pressure Ar and N_2 [12]. Both line parameters decreased faster in a N_2 atmosphere while, at the same linewidth values, the intensity was much lower in N_2. Similarly, a faster decrease in line intensity in N_2 or an air atmosphere has also been observed in other studies with different materials and different laser pulse lengths [8,16,17]. In our study [12], we proposed that the observed lower intensity in N_2 is caused by a lower plasma temperature and electron density resulting from the energy losses into N_2 dissociation and the excitation of many molecular excited states. In addition, the excited state of H could be quenched more efficiently by N_2 molecules. The rate of the latter process is proportional to the density of nitrogen molecules, and the importance of this effect of N_2 should decrease at lower pressures. However, the pressure and type of gas atmosphere also influence the formation and development of the plasma plume [10,18] and, therefore, may have a more complex influence on the H_α line intensity and linewidth.

Another observation from our earlier LIBS studies at atmospheric pressures was the difference in the spatial distribution of H_α and Mo I line intensity, with the H_α line intensity reaching maximum closer to the Mo target when compared to Mo I lines, which reached maximum intensity farther away from the target [13]. This effect was present in all investigated gases (Ar, He and N_2) and has also been observed in fs LIBS studies of Zircaloy-4 where Zr I lines reached maximum intensity farther away from the target when compared to the D line intensity [11,19]. This non-uniform spatial distribution has implications for the quantitative determination of elemental composition by the Calibration-Free LIBS (CF-LIBS) method [20,21], which relies on the spatial uniformity of the emitting species. Therefore, it is important to find the experimental conditions where the spatial distribution of H_α line and Mo I line intensities is more uniform.

The aim of the present study was to investigate the effect of the pressure of the Ar and N_2 atmosphere on the intensity and linewidth of the hydrogen H_α line. The line intensities were analyzed at different delay times between the laser pulse and spectral acquisition and at various distances along the plasma plume development axis. The 2D photos of the plasma plume at different delay times were also registered to investigate the development of integral emission and the shape of the plasma plume.

2. Materials and Methods

The investigations were carried out with a Mo disk with a 30 mm diameter and 2.5 mm thickness [12,13]. Similar Mo disks have been used as substrates for W coatings for plasma exposure studies in Magnum-PSI [22,23]. Mo is used as first wall material in EAST tokamak [6], as an interface layer between W divertor and carbon substrate in JET [24] and will be used as a material in in diagnostic mirrors of ITER [25]. The coating contains

0.5 at. % of hydrogen as a bulk impurity [12]. The percentage of hydrogen on the surface reached 4.7 at. % due to contamination by air moisture.

Figure 1 depicts the experimental setup that combines features from earlier studies [12,13]. The vacuum chamber was evacuated to a pressure below 10^{-3} mbar and then filled with argon or nitrogen with purity class 5.0 to the desired pressure in the 4 to 1000 mbar range. The pressure in the chamber was measured with a MKS instruments DualTransTM 910 Transducer.

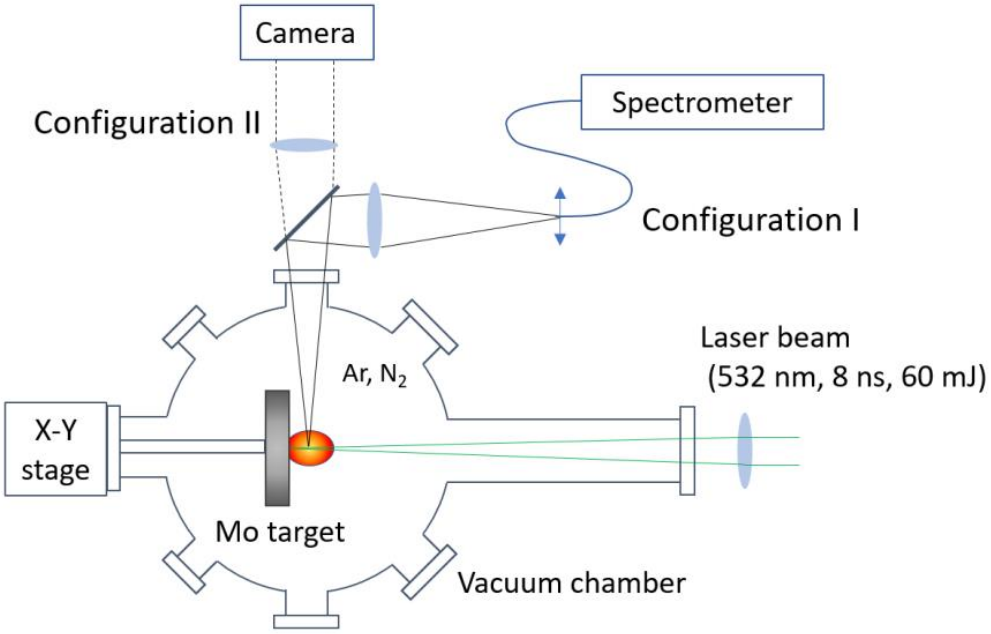

Figure 1. Schematic description of the experimental setup. The distance from the laser entrance window to the target was 80 cm and from the target to the side window was 30 cm.

The 8 ns laser pulse from a Quantel YG981C Nd:YAG laser was focused a few mm behind the Mo surface by a lens with a focal length of 150 cm. Such an arrangement was used to avoid a gas breakdown in front of the target. The laser pulse energy was 60 mJ, and the corresponding fluence at the target surface was approximately 15 J/cm^2. The pulse repetition rate was 1 Hz. Both the space-resolved photographs of the plasma plume and emission spectra originating from the plasma plume were collected perpendicular to the laser beam. The spatially resolved spectra were collected by focusing the plasma emission on a fiber that was connected to the Czerny-Turner type spectrometer LOMO MDR-23 (1200 grooves/mm grating) coupled with an Andor iStar340T iCCD camera. The apparatus function of the spectrometer determined by the He-Ne laser line at 632.8 nm was 0.06 nm. The magnification of this configuration was nearly 1:1, and the fiber diameter of 0.8 mm determined the spatial resolution of the spectrum recording. The delay time between the laser pulse and registration of the spectra varied from 0.2 to 10 µs. Three spectra were accumulated for each measurement condition for an improved signal-to-noise ratio.

The plume images were collected by the Andor iStar iCCD camera. A converging lens was set on the radiation path of the plasma plume to focus and slightly enlarged the image at the camera (magnification 1.3 times). Three different time series were used, each with 10 different delay times having steps of 50, 200 and 1000 ns and gate widths, respectively, of 20, 50 and 200 ns [12]. Each photo was the sum of five subsequent laser pulses.

Due to the limited surface area of the Mo sample and the large number of required measurements, the same spot on the sample was used for measurement series at different delay times and positions, while a new spot was used at each pressure value and gas type. First shots on the new surface site were not recorded to avoid the influence of

surface contamination, having different elemental concentrations and, therefore, the plasma plume properties.

3. Results

3.1. Plasma Plume Images

Photos recorded at different Ar and N_2 gas pressures and at various delay times are shown in Figure 2. Consistent with other studies [10,26,27], the pressure had a notable effect on the plume development. At the same time, the effect of the gas type remained less pronounced. At lower pressures, the plasma plume was more extensive, and the expansion lasted until the plume intensity diminished to the noise level. In addition, the plume had a reasonably well-defined front, resembling shockwave expansion, and the maximum intensity moved at some distance behind the plume front. At increasing pressures, the plume expansion became more confined, and, at the higher pressures, the expansion stopped at shorter delay times. At pressures 133 and 400 mbar, the plume became distorted with an additional bulge at the front of the plume. This distortion was less pronounced at the highest investigated pressure, 1000 mbar. The position of this bulge varied from shot to shot, both horizontally and vertically, and complicated the estimation of the dimensions of the plume. The formation of such features is also observed in other studies, and one possible cause for this bulge is the absorption of laser emissions in the gas phase at the front of the plume due to the preionization of the gas by previous laser shots [28–30]. However, in our study, the effect should be less pronounced due to the lower repetition rate and focusing the laser behind the target surface. Another possible reason for the perturbation at the interface of the plume front is the Rayleigh–Taylor instability [31,32].

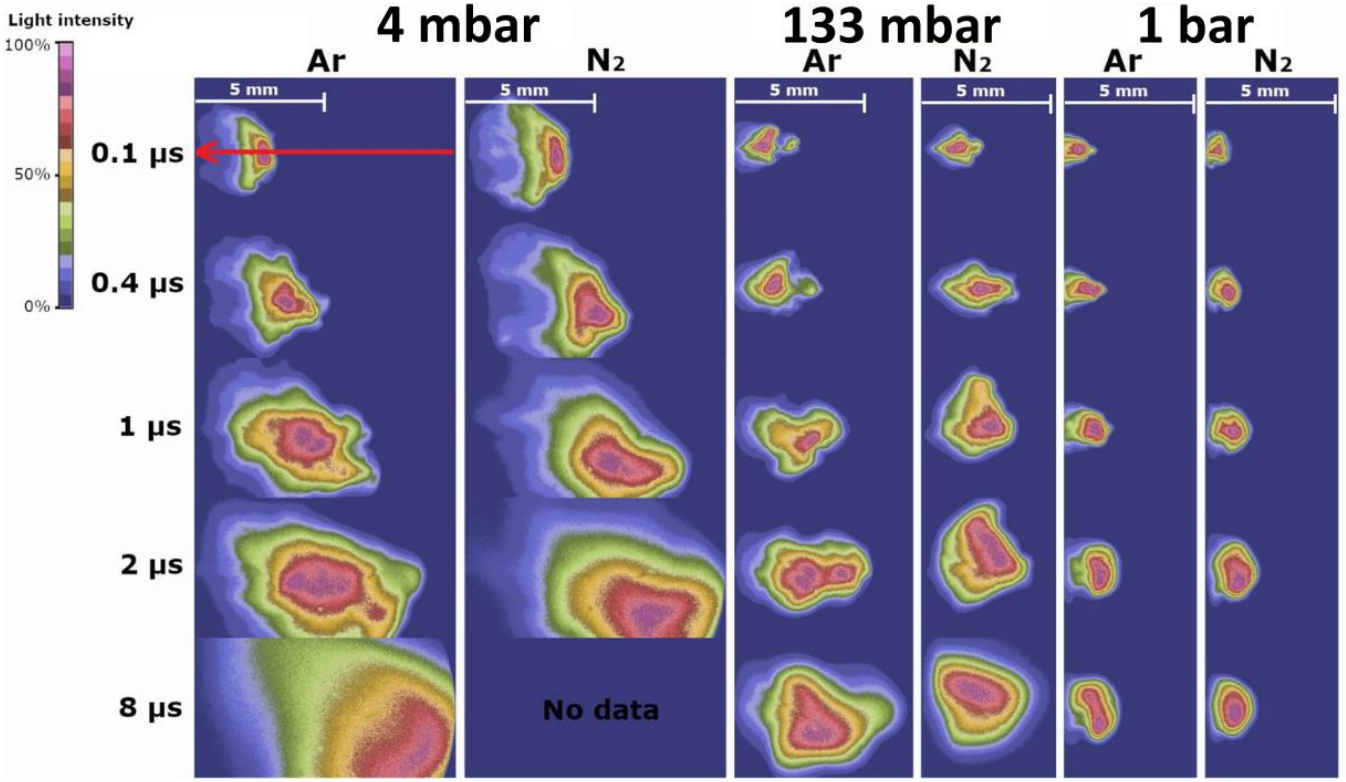

Figure 2. Photos of plasma plume intensity at different delay times and in Ar and N_2 environments at various pressures were recorded with configuration II. Each image was normalized to the maximum value. The target surface was at the left edge, and the laser beam originated from the right, as shown in the photo.

The plume front was defined by the intensity, which was at least 15% of the maximum intensity of the plume. The development of the plume front is shown in Figure 3 for Ar and N_2 atmospheres at different pressures. At pressures below 40 mbar, the plume front expanded until at least the distance of 10 mm, which was the maximum distance determined by the field of view of the camera. At these pressures, the plume expansion was approximately 15–20% faster in the case of nitrogen. At increasing pressures, the expansion started to stop at a certain distance, which occurred at somewhat lower pressures in the case of nitrogen. As discussed in the previous paragraph, a larger scatter in the distance value of plume front at 400 mbar pressure Ar is related to the formation of the bulge in the front of the plasma plume. A similar scatter was observed at 133 mbar both in Ar and N_2. The initial plume velocity determined from the slope of the first 3–4 measurement points of the distance, and the delay time reduced from about 6 mm/μs to 3 mm/μs with increasing pressure.

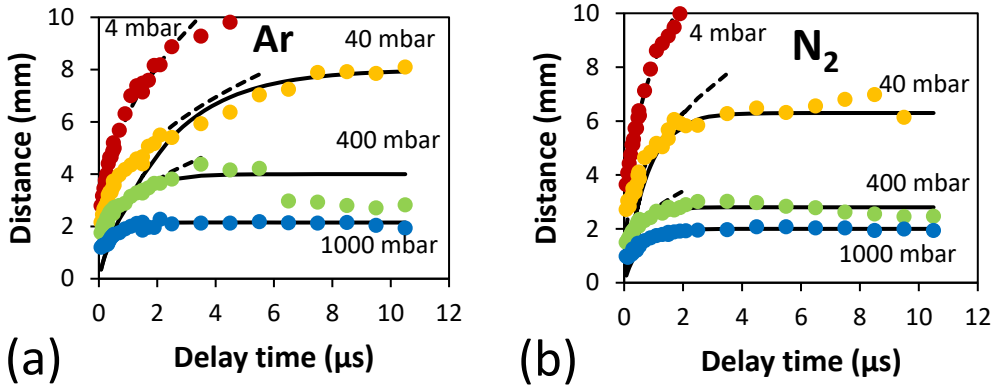

Figure 3. The distance of the plasma plume front as a function of delay time at different pressures of the (**a**) Ar and (**b**) N_2 atmosphere. The dashed lines show the theoretical distance calculated according to the shock model, and the solid line shows the calculation based on the drag model.

The findings are consistent with the results of other studies that have investigated plume expansion. At lower pressures, the plume front did not stop within the camera frame. The shock model based on the Taylor–Sedov theory was used to describe the time-dependent increase in the plume front distance $D = \xi_0 (E_0/\rho_0)^{1/5} t^{2/5}$ [26,31–33]. In this equation, E_0 is the laser pulse energy, ρ_0 is the background gas density, t is delay time and ξ_0 is a constant that depends on the ratio of the specific heats of the gas, which is 1.66 and 1.4 for Ar and N_2, respectively. The parameter $\xi_0 (E_0/\rho_0)^{1/5}$ determined by the fitting of the experimental curves at lower pressures scaled reasonably well with the ρ_0 calculated from the gas pressure. The parameter was approximately 15% larger in N_2 in comparison to Ar, while the constant ξ_0 should be approximately 10% larger in Ar. The reason for this discrepancy remains unclear.

At higher pressures and at longer delay times, there is a change from the shock (blast) model to the drag model: $D = D_0[1 - \exp(-\beta t)]$ [26,31–33]. In this equation, D_0 is the plume stopping distance, and β is the slowing coefficient, which is related to D_0 according to the relation $\beta = v_0/D_0$ with v_0 denoting the initial plume velocity. In our study, the drag model was applicable to the pressures down to 40 mbar. In the case of Ar, the value of β determined by the fitting of experimental data increased with the pressure from 0.5 to 2.5 μs^{-1}, which is consistent with the values calculated from the experimentally determined D_0 and the fixed initial plume velocity of 5 mm/μs. The latter value is comparable with the experimentally determined values. In the case of N_2, the β was higher than the predicted value. It should be noted that the determination of β was somewhat inaccurate due to the deviation from the model at shorter delay times and the scatter of experimental data.

The decay of the maximum intensity of the plasma plume at increasing delay times is shown in Figure 4a for different Ar pressures. Qualitatively similar dependencies were

observed in N_2 (Figure 4b), but the intensities were considerably lower in the latter case. For both gases, the maximum intensities increased with the gas pressure at all delay times until the pressure of 40 mbar. At shorter delay times and higher pressures, the intensity was not affected by the pressure as much, while, at longer delay times, above 1 µs, there were no clear trends in the intensity.

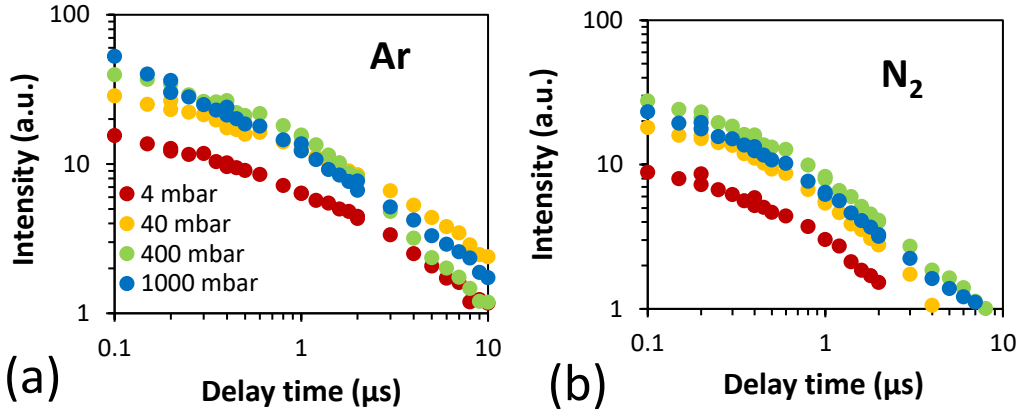

Figure 4. Delay time dependence of maximum intensity of the plasma plume images at different (**a**) Ar and (**b**) N_2 pressures. Red—4 mbar; Orange—40 mbar; Green—400 mbar; Blue—1000 mbar.

The ratio of maximum intensities of plasma plume in N_2 and Ar was 0.44–0.7 at delay times below 1 µs, and it decreased to 0.1–0.2 at the longest delay times and lower pressures (Figure 5). At the highest pressures, 400 and 1000 mbar, the ratio remained in the range of 0.4–0.7. Such differences in the plume intensities in Ar and N_2 were previously found at atmospheric pressures [12], where they were explained by the dissipation of a large fraction of laser pulse energy in N_2 to the dissociation and excitation of N_2 molecules. The results of the present study indicate that this effect influences the formation of plasma plumes at all investigated pressures. At low pressures, the intensity ratio further decreased in the later phase of the plume expansion. This change suggests that the plume expansion into the N_2 atmosphere resulted in additional energy losses. At higher pressures, the plume expansion stopped at about 1–2 µs, and the energy losses due to the mixing with N_2 atmosphere became smaller.

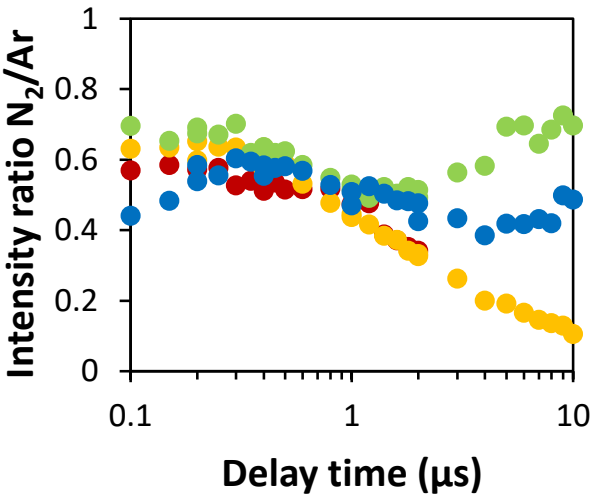

Figure 5. Delay time dependence of the ratio of maximum intensities in N_2/Ar at different pressures. Red—4 mbar; Orange—40 mbar; Green—400 mbar; Blue—1000 mbar.

3.2. Determination of H_α and Mo I Line Intensities

The following results are based on the spectra obtained with configuration I (Figure 1). Examples of the spectra obtained in Ar and N_2 atmospheres at 4 and 133 mbar are shown in Figure 6. These spectra feature an H_α line at 656.28 nm and several Mo I lines, with a prominent line at 661.91 nm (Figure 6a). There were also several notable lines that could not be identified based on the data available in openly accessible databases [34,35]. At certain experimental conditions, some of the lines overlapped with the H_α line and limited the accuracy of the determination of its intensity and Full Width at Half Maximum (FWHM) (Figure 6b). This problem occurred most notably at short delay times and in the plume region farther away from the target. The intensity and FWHM of the H_α line were determined by fitting the peak at 656.28 nm with the Lorentz profile, while the intensity of the Mo I line was determined by using the Gaussian profile. The FWHM value of the Gaussian profile was determined by the apparatus function of approximately 0.06 nm. The FWHM value of the Lorentz profile of the H_α line was determined by electron density through the Stark effect. At low pressures or longest delay times, the electron density was sufficiently small, and the line broadening of the H_α line was also mainly determined by the apparatus function.

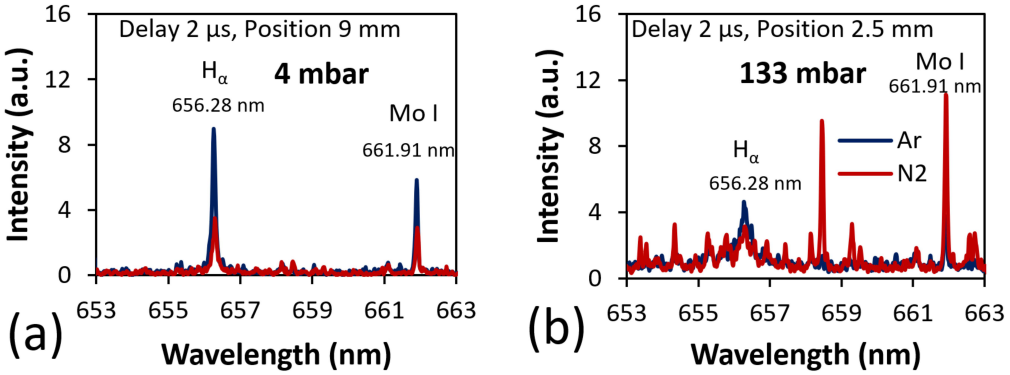

Figure 6. LIBS emission spectra around the 656 nm H_α line registered in the Ar and N_2 atmosphere at the (**a**) pressure of a 4 mbar delay time and a distance of 9 mm showing observed lines and (**b**) the pressure of 133 mbar and a distance of 2.5 mm showing overlapping and unidentified lines. The delay time was kept at 2 µs.

3.3. Spatial and Temporal Distribution of Hα and Mo I Line Intensities

Figure 7 shows the spatial and temporal distribution of the intensity of H_α line and the Mo I line at 661.91 nm in Ar and N_2 at different pressures. It should be noted that, at 1000 mbar, the measurements were made only at delay times starting from 1 µs because the H_α line could not be separated from other lines and the background intensity at shorter delay times due to the considerable broadening and interference from other lines. The main feature observable from the color maps is the different distribution of the intensity of the H_α and Mo lines. This difference was already observed in our previous study at atmospheric pressure [13], but the difference is also evident at lower pressures. The region with high H_α line intensity remained closer to the target surface, while the Mo line intensity reached high values farther away from the target. In addition, the H_α line intensity decreased monotonically already at the shortest delay times, while Mo line intensity reached maximum values at the delay times 1–2 µs depending on the gas pressure. The following reduction in Mo line intensity was also much slower, and, at the highest pressure, the intensity remained nearly the same for all investigated delay times. As a note, at the pressure of 133 mbar, the H_α line intensity diminished faster than at 4 or 1000 mbar, but its initial intensity was also considerably higher (see Section 3.4).

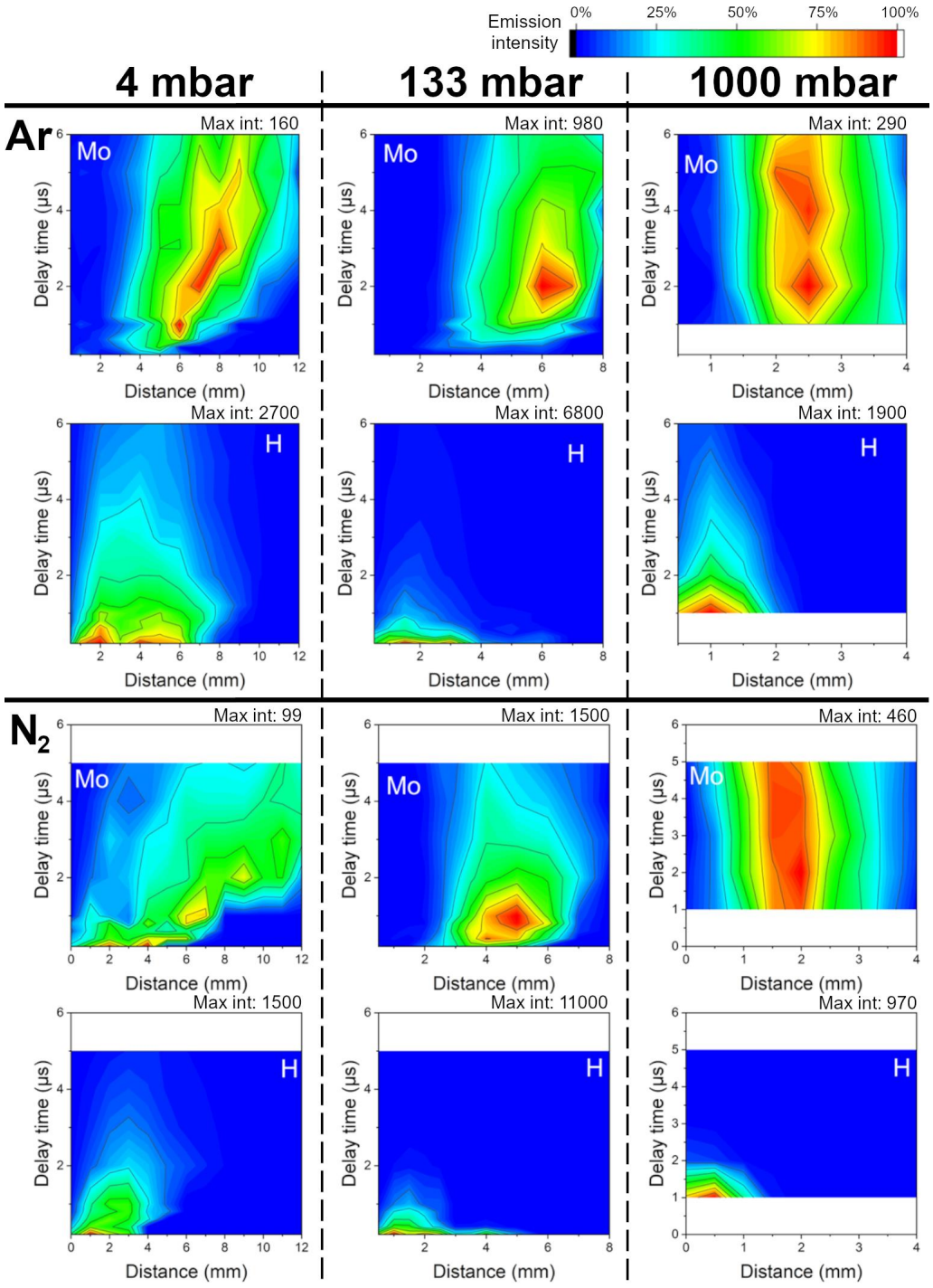

Figure 7. Two-dimensional color maps of the H_α and Mo I line intensities as a function of distance from the target and delay time. The maps are shown for Ar and N_2 at different pressures. Note the difference in the distance scale at various pressures. White regions show the lack of measurement results for these experimental conditions.

At lower pressures, the plasma plume expansion was evident from the time-dependent increase in the distance of Mo emission maximum and its farthest extent from the target. At higher pressures, there was practically no change in the intensity distribution at delay times longer than 1 μs due to the stopping plume expansion, and the region with strong emission was smaller. These results are consistent with the observations from the plume photos. In

the case of N_2, the H_α line diminished much more quickly, and its spatial distribution was considerably narrower and closer to the target surface.

The spatially different emission of H_α and Mo line intensities can be explained by different plasma conditions along the plasma plume. The temperature and plasma densities are expectedly higher in the central region of the plume [29], and this favors the excitation of the H (n = 3) state responsible for the H_α emission line. At the same time, the Mo atoms are mostly ionized in the central region of the plasma plume, and the emission of Mo atomic lines present in the wavelength region around 656 nm originates from the front of the plasma plume [29].

3.4. Time-Dependence of H_α Line Intensity and FWHM Values at the Emission Maximum

In the following comparison of the temporal evolution of H_α intensity in different gases and at various pressures, the intensities were spatially averaged over the region where the intensity was more than 50% of the maximum value. FWHM values of the H_α line were also averaged over the same region. Outside of this region, the accuracy of the line width determination was reduced, especially in the plume region with increased Mo line intensities, which overlapped with the H line (Figure 6b). As a practical implication, the LIBS experiments are usually made with a lower spatial resolution to obtain a stronger signal, and one can expect that this region of averaging gives the largest contribution to the H_α line.

The time-dependent changes in the averaged values of the H_α line intensity and FWHM are shown in Figure 8. At all pressures, the intensity and FWHM values decreased with the delay time, and, especially at long delay times, the decrease was faster in N_2. At short delay times, the difference in intensities and FWHM values was less pronounced between Ar and N_2, and, at 133 mbar, the values were the same in both gases up to the delay time of 1 μs. At these short delay times, the reduction rates, i.e., the speed of the decrease in line intensity and FWHM values were also higher. The qualitative change in the reduction rate occurred at about 0.4, 1 and 1.5 μs for the pressures 4, 133 and 1000 mbar, respectively. The intensity and FWHM values increased substantially in both gases when the pressure increased from 4 to 133 mbar. With the additional increase in the pressure to 1000 mbar, the intensities remained nearly the same in Ar, while the intensities decreased in N_2, especially at the later stages of the plume development.

The reduction rate constants k_1 and k_2 were determined by fitting the results with bi-exponential function $A_1\exp(-k_1 t) + A_2\exp(-k_2 t)$. Table 1 shows the reduction rate constant of the H_α line intensity k_2 corresponding to the longer delay times, where the differences between Ar and N_2 were most pronounced. The rate constants increased with the pressures and were 2.4–3 times higher in N_2. In our previous study [12], the higher reduction rate constant in N_2 was explained by the lower plasma temperature and density and the faster quenching of excited H (n = 3) states by nitrogen molecules. The latter effect should be proportional to the concentration of Ar and N_2 molecules. The reduction in the pressure by several orders of magnitude resulted only in a two-fold decrease in the rate coefficient, and this change mainly occurred at higher pressures. The quenching rate coefficients of Ar and N_2 are 4×10^{-10} cm^3/s and 20×10^{-10} cm^3/s. The density of gas atoms and molecules in the center of the plasma plume is not experimentally known, but, in our estimations, we assumed that the gas density in the plume center is an order of magnitude lower than in the surrounding gas [36,37]. The estimated quenching times were 0.5 and 0.1 ns at atmospheric pressure and 127 and 25 ns at 4 mbar of Ar and N_2, respectively. The lifetime of the H (n = 3) excited state was 17 ns. Consequently, the quenching is expected to become less important under low pressures. The faster reduction rate of H_α line intensity observed in N_2 at low pressures can, therefore, be explained by the reduction in the plasma temperature and density. The latter complies with the decrease in the ratio of the maximum plasma plume intensities in N_2 and Ar at longer delay times observed in Figure 5.

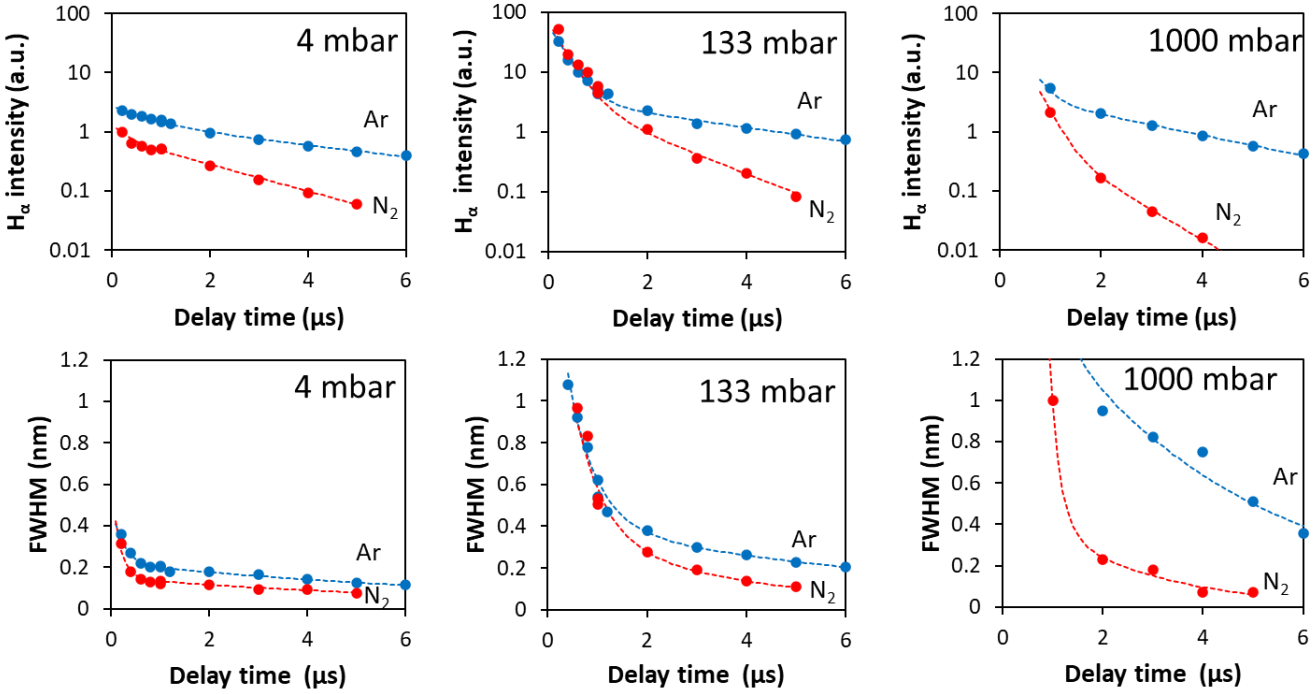

Figure 8. The distribution of H_α line intensity and FWHM along the axis of plasma plume development at different pressures of Ar and N_2. The delay time was kept at 2 μs. The dashed lines were obtained by fitting the experimental points with a bi-exponential function, which resulted in a reasonably good fit.

Table 1. The reduction rate constants k_2 of the H_α line intensity were determined at longer delay times for Ar and N_2. The units are $1/\mu s$.

Gas	Pressure		
	4 mbar	**133 mbar**	**1000 mbar**
Ar	0.22	0.27	0.4
N_2	0.52	0.75	1.15

3.5. Comparison of H_α Intensity and FWHM Values

For the quantification of the hydrogen isotopes, it is desirable to use the experimental conditions that result in the highest possible intensity at a sufficiently narrow line width. Both the intensity and FWHM values decreased with time as shown in Figure 8, and the optimum conditions may occur at different delay times for various gases and pressures. Figure 9 presents the H_α line intensity as a function of the FWHM value. Each point in a series determined for Ar and N_2 at a specific pressure corresponds to a measurement at a particular delay time. The gas pressure had the most decisive influence on the line intensity at a fixed FWHM. An intense but sufficiently narrow H_α line was obtained at lower pressures. Therefore, the use of lower pressure is advantageous for the distinguishing of the isotopes. However, the use of LIBS during the maintenance breaks of the reactors imposes limits on pressure reduction [4].

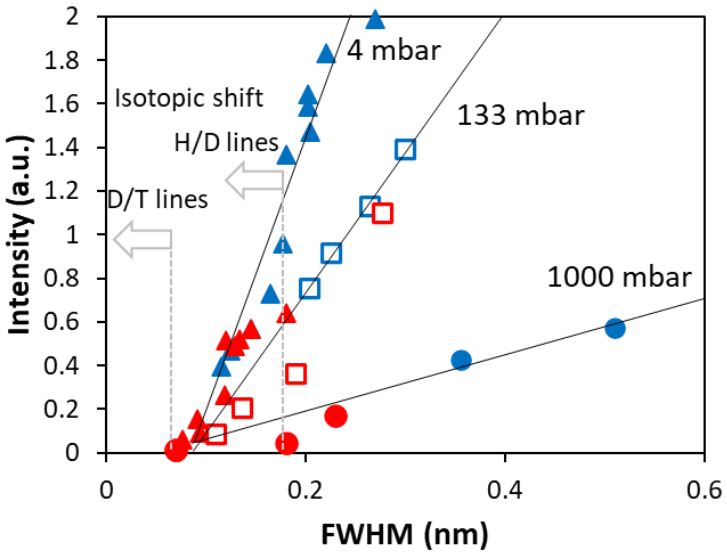

Figure 9. The averaged H_α line intensity as a function of the FWHM value for Ar and N_2 at different pressures. The dashed lines show the FWHM values corresponding to the isotopic shift in D and H or T and D lines. Filled triangles, empty squares and filled rings correspond to the pressures of 4 mbar, 133 mbar and 1000 mbar, respectively. The blue color corresponds to Ar, and the red color to N_2. The leftmost point for each pressure corresponds with a 6 µs delay time for Ar and a 5 µs delay time for N_2.

The gas used in the LIBS measurement influenced the intensities at FWHM values below 0.3 nm, corresponding to longer delay times (Figure 9). This difference became more pronounced at the increasing pressure as the ratio of intensity vs. FWHM slopes between Ar and N_2 increased and was approximately 1.3 times at 4 mbar, 1.9 times at 133 mbar and 2.3 times at 1000 mbar. In our previous study, we compared the relationship between intensity and FWHM in N_2 and Ar mixtures at atmospheric pressure (1000 mbar), and the difference between Ar and N_2 was considerably larger. The difference is explainable by the different optical setups used for the LIBS measurements. In the previous study, the emission was collected from about a 2–3 mm broad region of the plasma plume, and the same area was used for both gases. In the present study, we collected the emission from an approximately 1 mm wide region for better spatial resolution. According to the present results at atmospheric pressure, the size of the emitting region was about 2 mm in Ar and 1 mm in N_2. Even when the average emission intensity at the same FWHM value is the same for both gases, the total collected emission intensity is higher when the emission is collected from a larger plume region. Another factor that can influence the H_α line intensity is the position where the emission is collected. In the case of Ar, the position of the maximum is at about 1 mm from the target surface, while, in N_2, the position is at the target surface. The position where the light was collected was optimized according to the maximum total intensity in the Ar. At the same distance, the H_α line intensity was considerably lower in N_2.

4. Conclusions

The present study investigated the effect of gas pressure in Ar and N_2 on the plasma plume and H_α line intensity. According to the plume images, the plasma plume grew faster and expanded farther at lower pressures, and the plume dimensions were similar in both gases. The maximum intensity of the plasma emission reached the highest values with medium pressures, and the intensity was considerably lower in N_2. This finding is one of the reasons why pressures below atmospheric pressure are beneficial for intensity measurements.

There was a remarkable difference in the spatial distribution of H_α and Mo I line intensity. This difference was more pronounced at lower pressures and longer delay times.

The difference was more significant in N_2, where the H_α line intensity reached maximum values closer to the target surface than in Ar. When the LIBS optical setup collects the emission along the axis of plume development, the collected emission of H_α and Mo lines originate at different plasma regions, which have different plasma conditions. This nonuniform distribution has implications for quantifying hydrogen isotope concentrations by CF-LIBS, which requires a uniform spatial distribution of the emitting species.

At longer delay times, the H_α line intensity and FWHM values decreased faster in N_2, while, at the shortest delay times, the difference was smaller or negligible. This difference was present at all pressures. Since both the H_α line intensity and FWHM values decreased faster in N_2, it was necessary to compare the H_α intensity values at the delay times, which resulted in the same FWHM value. This comparison showed that, at small FWHM values corresponding to longer delay times, the intensity was clearly smaller in N_2, but the difference in intensity to the FWHM ratio was less pronounced, especially at the low pressure of 4 mbar. The results further highlighted the importance of optimizing the optical setup of the LIBS system for the gas atmosphere because the region with the highest intensity of the H_α line varied with pressure and gas type.

Lower gas pressure would be advantageous for H isotope measurements due to the higher intensity of isotope lines at the same FWHM values. However, the pressure must be reduced several times to have a considerable effect on the intensity. When the pressure is reduced by pumping the atmosphere in the confined volume of the LIBS system on a remote arm, such as that used in the FTU, the resulting low-pressure atmosphere contains nitrogen or air. According to present results, the intensities remained lower in nitrogen even at lower pressure, and, therefore, the positive effect of lower pressure will be less pronounced.

Author Contributions: Conceptualization, I.J. and P.P.; methodology, P.P.; software, J.R.; validation, I.J. and J.R.; formal analysis, I.J and J.R.; investigation, P.P and J.R.; resources, I.J and P.P.; data curation, I.J., J.R. and P.P.; writing—original draft preparation, I.J.; writing—review and editing, I.J., J.R. and P.P.; visualization, I.J. and J.R.; supervision, I.J.; project administration, I.J.; funding acquisition, I.J. and P.P. All authors have read and agreed to the published version of the manuscript.

Funding: This work was carried out within the framework of the EUROfusion Consortium, funded by the European Union via the Euratom Research and Training Programme (Grant Agreement No 101052200—EUROfusion). Views and opinions expressed are, however, those of the author(s) only and do not necessarily reflect those of the European Union or the European Commission. Neither the European Union nor the European Commission can be held responsible for them.

Data Availability Statement: Dataset is available upon request from the authors.

Conflicts of Interest: The authors declare no conflicts of interest. The funders had no role in the design of this study; in the collection, analyses, or interpretation of data; in the writing of the manuscript; or in the decision to publish the results.

References

1. Girard, J.P.; Garin, P.; Taylor, N.; Uzan-Elbez, J.; Rodríguez-Rodrigo, L.; Gulden, W. ITER, safety and licensing. *Fusion. Eng. Des.* **2007**, *82*, 506–510. [CrossRef]
2. Lukacs, M.; Williams, L.G. Nuclear safety issues for fusion power plants. *Fusion. Eng. Des.* **2020**, *150*, 111377. [CrossRef]
3. Philipps, V.; Malaquias, A.; Hakola, A.; Karhunen, J.; Maddaluno, G.; Almaviva, S.; Caneve, L.; Colao, F.; Fortuna, E.; Gasior, P.; et al. Development of laser-based techniques for in situ characterization of the first wall in ITER and future fusion devices. *Nucl. Fusion.* **2013**, *53*, 093002. [CrossRef]
4. Van Der Meiden, H.J.; Almaviva, S.; Butikova, J.; Dwivedi, V.; Gasior, P.; Gromelski, W.; Hakola, A.; Jiang, X.; Jõgi, I.; Karhunen, J.; et al. Monitoring of tritium and impurities in the first wall of fusion devices using a LIBS based diagnostic. *Nucl. Fusion.* **2021**, *61*, 125001. [CrossRef]
5. Semerok, A.; Grisolia, C. LIBS for tokamak plasma facing components characterisation: Perspectives on in situ tritium cartography. *Nucl. Instrum. Methods Phys. Res. A* **2013**, *720*, 31–35. [CrossRef]
6. Hu, Z.; Gierse, N.; Li, C.; Liu, P.; Zhao, D.; Sun, L.; Oelmann, J.; Nicolai, D.; Wu, D.; Wu, J.; et al. Development of laser-based technology for the routine first wall diagnostic on the tokamak EAST: LIBS and LIAS. *Phys. Scr.* **2017**, *2017*, 014046. [CrossRef]
7. Almaviva, S.; Caneve, L.; Colao, F.; Lazic, V.; Maddaluno, G.; Mosetti, P.; Palucci, A.; Reale, A.; Gasior, P.; Gromelski, W.; et al. LIBS measurements inside the FTU vacuum vessel by using a robotic arm. *Fusion. Eng. Des.* **2021**, *169*, 112638. [CrossRef]

8. Maddaluno, G.; Almaviva, S.; Caneve, L.; Colao, F.; Lazic, V.; Laguardia, L.; Gasior, P.; Kubkowska, M. Detection by LIBS of the deuterium retained in the FTU toroidal limiter. *Nucl. Mater. Energy* **2019**, *18*, 208–211. [CrossRef]
9. Favre, A.; Bultel, A.; Sankhe, M.L.; Vartanian, S.; Bruno, V.; Morel, V.; L'Hermite, D.; Sirven, J.B.; Diez, M.; Missirlian, M.; et al. A step towards the diagnostic of the ITER first wall: In-situ LIBS measurements in the WEST tokamak. *Phys. Scr.* **2024**, *99*, 035609. [CrossRef]
10. De Giacomo, A.; Dell'Aglio, M.; Gaudiuso, R.; Amoruso, S.; De Pascale, O. Effects of the background environment on formation, evolution and emission spectra of laser-induced plasmas. *Spectrochim. Acta Part B Spectrosc.* **2012**, *78*, 1–19. [CrossRef]
11. Kautz, E.J.; Rönnebro, E.C.E.; Devaraj, A.; Senor, D.J.; Harilal, S.S. Detection of hydrogen isotopes in Zircaloy-4: Via femtosecond LIBS. *J. Anal. Spectrom.* **2021**, *36*, 1217–1227. [CrossRef]
12. Jõgi, I.; Ristkok, J.; Raud, J.; Butikova, J.; Mizohata, K.; Paris, P. Laser induced breakdown spectroscopy for hydrogen detection in molybdenum at atmospheric pressure mixtures of argon and nitrogen. *Fusion. Eng. Des.* **2022**, *179*, 113131. [CrossRef]
13. Jõgi, I.; Ristkok, J.; Butikova, J.; Raud, J.; Paris, P. LIBS plasma in atmospheric pressure argon, nitrogen and helium: Spatio-temporal distribution of plume emission and Hα linewidth. *Nucl. Mater. Energy* **2023**, *37*, 101543. [CrossRef]
14. Idris, N.; Kurniawan, H.; Lie, T.J.; Pardede, M.; Suyanto, H.; Hedwig, R.; Kobayashi, T.; Kagawa, K.; Maruyama, T. Characteristics of hydrogen emission in laser plasma induced by focusing fundamental Q-sw YAG laser on solid samples. *Jpn. J. Appl. Phys. Part 1 Regul. Pap. Short Notes Rev. Pap.* **2004**, *43*, 4221–4228. [CrossRef]
15. Almaviva, S.; Caneve, L.; Colao, F.; Lazic, V.; Maddaluno, G.; Mosetti, P.; Palucci, A.; Reale, A.; Gasior, P.; Gromelski, W.; et al. LIBS measurements inside the FTU vessel mock-up by using a robotic arm. *Fusion. Eng. Des.* **2020**, *157*, 111685. [CrossRef]
16. Paris, P.; Butikova, J.; Laan, M.; Aints, M.; Hakola, A.; Piip, K.; Tufail, I.; Veis, P. Detection of deuterium retention by LIBS at different background pressures. *Phys. Scr.* **2017**, *T170*, 014003. [CrossRef]
17. Mittelmann, S.; Touchet, K.; Mao, X.; Park, M.; Brezinsek, S.; Pretzler, G.; Zorba, V. Hydrogen isotope analysis in W-tiles using fs-LIBS. *Sci. Rep.* **2023**, *13*, 2285. [CrossRef]
18. Capitelli, M.; Casavola, A.; Colonna, G.; De Giacomo, A. Laser-induced plasma expansion: Theoretical and experimental aspects. *Spectrochim. Acta Part B Spectrosc.* **2004**, *59*, 271–289. [CrossRef]
19. Kautz, E.J.; Devaraj, A.; Senor, D.J.; Harilal, S.S. Hydrogen isotopic analysis of nuclear reactor materials using ultrafast laser-induced breakdown spectroscopy. *Opt. Express* **2021**, *29*, 4936. [CrossRef]
20. Ciucci, A.; Corsi, M.; Palleschi, V.; Rastelli, S.; Salvetti, A.; Tognoni, E. New procedure for quantitative elemental analysis by laser-induced plasma spectroscopy. *Appl. Spectrosc.* **1999**, *53*, 960–964. [CrossRef]
21. Tognoni, E.; Cristoforetti, G.; Legnaioli, S.; Palleschi, V. Calibration-Free Laser-Induced Breakdown Spectroscopy: State of the art. *Spectrochim. Acta Part B Spectrosc.* **2010**, *65*, 1–14. [CrossRef]
22. Jõgi, I.; Paris, P.; Piip, K.; Ristkok, J.; Talviste, R.; Piirsoo, H.M.; Tamm, A.; Grigore, E.; Hakola, A.; Tyburska-Pueschel, B.; et al. LIBS applicability for investigation of re-deposition and fuel retention in tungsten coatings exposed to pure and nitrogen-mixed deuterium plasmas of Magnum-PSI. *Phys. Scr.* **2021**, *96*, 114010. [CrossRef]
23. Paris, P.; Jõgi, I.; Piip, K.; Passoni, M.; Dellasega, D.; Grigore, E.; Arnoldbik, W.M.; van der Meiden, H. In-situ LIBS and NRA deuterium retention study in porous W-O and compact W coatings loaded by Magnum-PSI. *Fusion. Eng. Des.* **2021**, *168*, 23–27. [CrossRef]
24. Likonen, J.; Coad, J.P.; Alves, E.; Catarino, N.; Coffey, I.; Krat, S.; Mayer, M.; Mizohata, K.; Widdowson, A. Material transport from marker tiles in the JET divertor. *Nucl. Mater. Energy* **2023**, *36*, 101505. [CrossRef]
25. Rubel, M.; Moon, S.; Petersson, P.; Widdowson, A.; Pitts, R.A.; Aleiferis, S.; Fortuna-Zaleśna, E.; De Temmerman, G.; Reichle, R. First mirror erosion-deposition studies in JET using an ITER-like mirror test assembly. *Nucl. Fusion.* **2021**, *61*, 046022. [CrossRef]
26. Aguilera, J.A.; Aragón, C. Temperature and electron density distributions of laser-induced plasmas generated with an iron sample at different ambient gas pressures. *Appl. Surf. Sci.* **2002**, *197–198*, 273–280. [CrossRef]
27. Mercadier, L.; Hermann, J.; Grisolia, C.; Semerok, A. Analysis of deposited layers on plasma facing components by laser-induced breakdown spectroscopy: Towards ITER tritium inventory diagnostics. *J. Nucl. Mater.* **2011**, *415*, S1187–S1190. [CrossRef]
28. Mercadier, L.; Hermann, J.; Grisolia, C.; Semerok, A. Diagnostics of nonuniform plasmas for elemental analysis via laser-induced breakdown spectroscopy: Demonstration on carbon-based materials. *J. Anal. Spectrom.* **2013**, *28*, 1446–1455. [CrossRef]
29. Aguilera, J.A.; Bengoechea, J.; Aragón, C. Spatial characterization of laser induced plasmas obtained in air and argon with different laser focusing distances. *Spectrochim. Acta Part B Spectrosc.* **2004**, *59*, 461–469. [CrossRef]
30. Kautz, E.J.; Senor, D.J.; Harilal, S.S. The interplay between laser focusing conditions, expansion dynamics, ablation mechanisms, and emission intensity in ultrafast laser-produced plasmas. *J. Appl. Phys.* **2021**, *130*, 204901. [CrossRef]
31. Sharma, A.K.; Thareja, R.K. Plume dynamics of laser-produced aluminum plasma in ambient nitrogen. *Appl. Surf. Sci.* **2005**, *243*, 68–75. [CrossRef]
32. Farid, N.; Harilal, S.S.; Ding, H.; Hassanein, A. Emission features and expansion dynamics of nanosecond laser ablation plumes at different ambient pressures. *J. Appl. Phys.* **2014**, *115*, 033107. [CrossRef]
33. Singh, R.P.; Gupta, S.L.; Thareja, R.K. Optical probe investigation of laser ablated carbon plasma plume in nitrogen ambient. *Phys. Plasmas* **2013**, *20*, 123509. [CrossRef]
34. Kramida, A.; Ralchenko, Y.; Reader, J.; NIST ASD Team. *NIST Atomic Spectra Database (Ver. 5.11)*; National Institute of Standards and Technology: Gaithersburg, MD, USA, 2024. Available online: https://physics.nist.gov/asd (accessed on 5 November 2024).

35. Kurucz, R.L.; Bell, B. *Atomic Line Data, Kurucz CD-ROM No.23*; Smithsonian Astrophysical Observatory: Cambridge, MA, USA, 1995.
36. Bogaerts, A.; Chen, Z.; Bleiner, D. Laser ablation of copper in different background gases: Comparative study by numerical modeling and experiments. *J. Anal. Spectrom.* **2006**, *21*, 384–395. [CrossRef]
37. Colonna, G.; Pascazio, G.; Bonelli, F. Advanced model for the interaction of a Ti plume produced by a ns-pulsed laser in a nitrogen environment. *Spectrochim. Acta Part B Spectrosc.* **2021**, *179*, 106120. [CrossRef]